Published in final edited form as:
Matrix Biol. 2008 July ; 27(6): 573–585. doi:10.1016/j.matbio.2008.02.008.

Fibroblast-derived 3D matrix differentially regulates the growth and drug-responsiveness of human cancer cells

Ilya Serebriiskii, **Remedios Castelló-Cros**, **Acacia Lamb**, **Erica A. Golemis***, and **Edna Cukierman***

Division of Basic Science/Tumor Cell Biology, Fox Chase Cancer Center, 333 Cottman Ave., Philadelphia, PA 19111.

Abstract

Recent studies have emphasized the importance of cellular microenvironment in modulating cell growth and signaling. *In vitro*, collagen matrices, Matrigel, and other synthetic support systems have been used to simulate *in vivo* microenvironments, and epithelial cells grown in these matrices manifest significant differences in proliferation, differentiation, response to drugs, and other parameters. However, these substrates do not closely resemble the mesenchymal microenvironment that is typically associated with advanced carcinomas *in vivo*, which is produced to a large extent by fibroblasts. In this study, we have evaluated the ability of a fibroblast-derived three-dimensional matrix to regulate the growth of a panel of 11 human tumor epithelial cell lines. Although proliferative and morphological responses to three-dimensional cues segregated independently, general responsiveness to the matrix correlated with the ability of matrix to influence drug responses. Fibroblast-derived three-dimensional matrix increased β1-integrin-dependent survival of a subset of human cancer cell lines during taxol treatment, while it sensitized or minimally influenced survival of other cells. β1-integrin-dependent changes in cell resistance to taxol did not correlate with degree of modulation of FAK and Akt, implying additional signaling factors are involved. Based on these results, we propose these matrices potentially have value as *in vitro* drug screening platforms.

Keywords

extracellular matrix; drug response; fibroblast; cancer cell; three-dimensional matrix; microenvironment; taxol; β1-integrin and tumor-stroma

Introduction

Epithelial cells, which give rise to the majority of solid tumors, are surrounded proximally by a thin protein matrix termed the basement membrane, and distally by a mesenchymal stroma rich in fibroblasts that secretes a mesh of proteins termed the extracellular matrix (ECM). It is now known that cancer initiation and progression are characterized by dynamic changes in signaling between the stroma and embedded tumor cells (Bissell and Labarge, 2005; Bissell et al., 2002; Muller, 2004; Soto and Sonnenschein, 2005). As tumors grow, stromal fibroblasts

*Corresponding authors, Fox Chase Cancer Center, 333 Cottman Ave., Philadelphia, PA 19111-2497, Phone: 215-214-4218 (EC), 215-728-2860 (EG), Fax: 215-728-3616, Emails: Edna.Cukierman@fccc.edu and Erica.Golemis@fccc.edu.
Please send reprint requests to E. Cukierman, see above address.

undergo changes in morphology, organization and expression of specific proteins, such as smooth muscle actin (Chaponnier and Gabbiani, 2004; Desmouliere et al., 2004). These changes render the fibroblasts “permissive”, actively promoting tumor cell growth and allowing the tumors to lose contact inhibition and become invasive (Mareel and Leroy, 2003). As the tumor cells gain greater access to the mesenchymal stroma (Bhowmick et al., 2004; Park et al., 2000), the basement membrane is concurrently degraded (Amenta et al., 2003; Yang et al., 2004).

To build more physiological *in vitro* systems to analyze the characteristics of cancer progression, it is becoming common to grow cancer cells within three-dimensional (3D) synthetic support systems that attempt to simulate a natural microenvironment, rather than on tissue culture plastic (Fischbach et al., 2007; Kim, 2005; Yamada and Cukierman, 2007). Such matrices include Matrigel (produced by EHS tumors, (Kleinman et al., 1986)), polymerized collagen (Grinnell et al., 2006; Grinnell et al., 1989), and other synthetic media (e.g., (Hwang et al., 2006)). Clearly, these matrices can regulate the growth of tumor cells in many ways, affecting their proliferation, morphology, survival signaling, invasive potential and response to chemotherapeutic agents (Griffith and Swartz, 2006). However, Matrigel is most comparable to the gel-like composition of basement membrane, which is rich in laminin, collagen IV, perlecan and other non-fibrous matrix components (Kleinman and Martin, 2005), rather than the fibrous mesh that characterizes a mesenchymal stroma, in which fibrous polymeric matrix proteins such as fibronectin and collagens III and I predominate (Desmouliere et al., 2004). While it is possible to roughly simulate the 3D fibrous nature of a mesenchymal stroma using a pure preparation of collagen I or other pure protein populations, such wholly defined systems lack numerous proteins, hormones, and other small molecule constituents of stromal matrix (Cukierman et al., 2002; Yamada and Cukierman, 2007). Hence, although these matrices may regulate tumor cell growth, any observed effect is not necessarily comparable to that produced by a fibroblast-rich stroma. Moreover, a plethora of reports have suggested that the thinning or degradation of basement membranes at early stages of tumor development is a frequent event (Akashi et al., 2005; Capo-Chichi et al., 2002; Netto et al., 2006). This early basement membrane degradation facilitates a more direct contact between the neoplastic epithelial cells and the adjacent mesenchymal compartments. Further, fibroblasts have been shown to invade the tumor mass and to produce and alter the tumor ECM, which is used by the epithelial cells for growth support and as pre-intravasation microenvironments (Condeelis and Segall, 2003). Together, these observations suggest that using *in vivo*-like mesenchymal matrices may represent a more accurate way to mimic *in vivo* microenvironments, providing an advantage over 2D cultures in assessing the physiological growth properties of tumor cells.

The recent development of fibroblast-derived 3D matrices (Beacham et al., 2006; Cukierman, 2002; Cukierman, 2005; Cukierman et al., 2001), and the determination that these matrices can actively regulate the growth of naïve fibroblasts re-plated within these matrices (Amatangelo et al., 2005; Cukierman et al., 2001; Damianova et al., 2007; Pankov et al., 2005), has the potential to produce a new and physiological assay system with which to study tumor growth. In this study we have examined the changes in the proliferation rate and morphology of a panel of epithelial tumor cell lines induced by fibroblast-derived 3D matrix. In addition, it has long been known that tumor cells grown in 3D environments differ in their susceptibility to chemotherapeutic agents from cells grown on 2D (Frankel et al., 1997; Hazlehurst et al., 2003; Morin, 2003; Zahir and Weaver, 2004). Using our system, we have compared the sensitivity of tumor cell lines to a set of chemotherapeutic drugs with the general propensity of these cells to have their morphology and proliferation rates regulated by the 3D matrix, as well as their propensity to basal or drug-induced apoptosis. Importantly, the level of responsiveness that a given epithelial cell line presented when cultured on *in vivo*-like mesenchymal matrix correlated with tendency to a 3D matrix-dependent drug response (e.g., for taxol). Moreover, as opposed to previous observations testing matrix-induced drug

resistance in 2D (Aoudjit and Vuori, 2001), this 3D matrix-induced resistance also depends on β1-integrin activity, but does not require activation of the serine/threonine protein kinase Akt/PKB. In sum, these data offer a proof-of-concept experiment, potentially supporting the expanded use of fibroblast-derived 3D matrices as an *in vitro* platform for assessment of drug activity.

Results

Human tumor cell lines respond differently to fibroblast-derived 3D matrix

To assess the role of fibroblast-derived 3D matrix in regulating the proliferation of tumor cells, we assembled a panel of 10 human tumor cell lines and 1 immortalized non-tumorigenic control line (Table 1). These were cultured in 96 well plates in triplicate, either directly on tissue culture plastic or on NIH3T3-derived 3D matrices. Cells were grown for 3 days, and growth curves established. The merged results of three independent experiments are shown in Figures 1A and B. Growth on fibroblast-derived 3D matrix severely inhibited the proliferation rate of some of the cell lines (e.g., NCI-H460 cells almost ceased to grow), and moderately inhibited the growth of some additional cell lines, such as MCF7 and PA-1. In contrast, the proliferation of some cell lines was essentially unaffected by growth on 3D matrix (e.g. COLO 205, SW620), while the PANC-1 cell line grew slightly better on the matrix.

Use of fibroblast-derived matrix differs from classic tissue culture not only in providing a 3D growth environment, but also in its specific protein and growth factor content. We asked whether the phenotypes we observed represent cellular response specifically to 3D fibroblast matrix, or to protein and growth factor cues provided in 2D. To do so, 4 cell lines with different response profiles for proliferation (NCI-H460, HCT116, PA-1, and COLO 205) were selected. These cells were re-plated in parallel on tissue culture plastic or on plates coated with solubilized fibroblast-derived matrix (Beacham et al., 2006; Cukierman et al., 2001; Cukierman et al., 2002), which had the same protein composition as 3D matrix, but presented to the cells as a 2D substrate (Figure 1C). Cells grew comparably on plastic and 2D matrix, indicating the proliferation response seen was specific to matrix proteins presented in a 3D conformation.

We next assessed changes induced in the morphology of the 11 cell lines by plating them onto 3D matrices or 2D tissue culture plastic (see Figure 2A for representative examples and Supplemental Figure 1 for the remaining cell lines). As with proliferative response, the morphology of some cells was strongly influenced by growth on 3D matrix, while other cell lines were indifferent to the type of substrate used. At 2 days after plating, some cell lines, including most notably PA-1 cells, responded to 3D matrices by assuming a spindle fibroblast-like morphology (see PA-1 on 3D matrix in Figure 2). A lesser, but still clear, spindle morphology was seen with HS 578T and some additional cell lines (Supplemental Figure 1). In contrast, other cell lines became notably rounded or amoeboid like. These included NCI-H460 (Figure 2), HCT116(p53−/−), and PANC-1 (Supplemental Figure 1). Finally, two cell lines, including COLO 205 (Figure 2) and SW620 (Supplemental Figure 1), were morphologically unresponsive to matrix. As a control, we also assessed the effect that solubilized 2D matrix has on the morphology of selected cell lines. The appearance of NCI-H460, PA-1, and COLO 205 cells plated onto 2D matrix mix was not affected in comparison to the morphology of these cells plated onto classic 2D culture plastic (see these examples in Figure 3 and compare with Figure 2). This observation indicates that, as with proliferation, the matrix only induced morphological changes when its proteins were displayed in a mesenchymal cell-organized 3D context.

To determine whether the ability of 3D matrix to induce morphological and proliferative effects correlated, or varied independently, we classified the degree of these responses as negligible (0), weak (1), moderate (2) or strong (3), and plotted them for each cell line (Figure 4). Based

on this analysis, the responsiveness of cell lines to fibroblast-derived 3D matrix varied independently for growth and morphology. For example, PA-1 cells had a strong morphological response to matrix but almost no observed effect on proliferation, while the NCI-460 proliferation rate was greatly reduced by 3D matrix, but the morphology of these cells was only moderately affected. The matrix affected neither the proliferation nor the morphology of two of the cell lines, COLO 205 and SW620.

Fibroblast 3D matrix induces specific responses to taxol. We next evaluated whether fibroblast-derived 3D matrix could influence the responsiveness (e.g., resistance or sensitivity) of cells to drugs targeting specific signal transduction pathways, as well as to general cytotoxic agents. For this purpose, we selected the PANC-1 pancreatic cancer cell line, as both the morphology and proliferation rate of this line were moderately affected by the 3D matrix (Figure 4). We selected a set of 5 protein-targeted or cytotoxic agents for this analysis (Table 1), and confirmed that these inhibited the proliferation of PANC-1 cells grown on classic tissue culture plastic, with 50% inhibition of growth (IC50) at μM or lesser concentrations. Using these 5 compounds, we performed IC50 curves in PANC-1 cells grown onto 3D matrix and compared these values to the IC50 values obtained with PANC-1 cells grown on plastic (Figure 5, A to E). Analysis of the relative IC50 values for these growth conditions revealed that for 4 of the compounds (MCP1, Gefitinib (Iressa), sorafenib (Nexavar), and imatinib (Gleevec)), the IC50 values observed were comparable on the two substrates. Notably, taxol was 4-fold less effective in inhibiting PANC-1 cell growth on 3D matrix in comparison to the growth inhibition obtained on plastic (Figure 5F).

The fact that PANC-1 cells became resistant to taxol when cultured on 3D matrix suggested that resistance could directly be related to relative growth rate of the cells, as matrix slightly stimulated the growth of PANC-1 cells (Figure 1A). An alternative possibility was that fibroblast 3D matrix might regulate the predilection of cells to resist apoptosis. To test this, we assessed the basal and taxol-stimulated incidence of apoptosis of PANC-1 cells on 3D matrix or 2D plastic (Figure 5, G to I). The basal rate of apoptosis was similarly low in PANC-1 cells grown on plastic or 3D matrix, and treated with low dose (10 nM) taxol. However, at higher doses of taxol (50 and 100 nM), PANC-1 cells grown on plastic underwent apoptosis at 3–5 fold higher rates than those grown on 3D matrix. These results suggest that, indeed, lower apoptosis rates in cells cultured onto 3D matrix could account for the observed 3D matrix induced resistance of PANC-1 cells to taxol.

We next asked if the observed resistance to taxol depended on the 3D matrix configuration versus the matrix composition present in 2D, and also if the matrix-associated drug resistance was specific to PANC-1 cells or whether it was also found in additional cell lines. For this purpose, we tested the response to taxol in 4 other cell lines grown either on 3D matrix, or plated on 2D matrix mix or 2D plastic controls. HS 578T breast carcinoma and PA-1 ovarian teratocarcinoma cells were selected since 3D matrix induced both proliferative and morphological effects in these lines that were opposite to the effects seen in PANC-1 (Figure 4). For comparison, COLO 205 and SW620 human colorectal adenocarcinoma cells were selected as reference cell lines where 3D matrix induced no proliferative or morphological effects (see Figure 4). Figure 5J indicates that like PANC-1 cells, HS 578T cells experienced a 3D matrix-dependent resistance to taxol that was not observed in 2D matrix. Intriguingly, PA-1 cells experienced a slight 3D-matrix-dependent sensitization to taxol, which was not evident in 2D matrix. Finally, for COLO 205 and SW620 cells, response to taxol was not influenced by growth in 3D or 2D matrix.

Fibroblast 3D matrix-induced taxol responses depend on β1-integrin but not Akt/PKB, FAK, or NF-κB

We next investigated the mechanisms responsible for the observed matrix-induced taxol resistance in matrix-responsive (e.g., PANC-1, HS 578T, and PA-1) versus unresponsive (e.g., COLO 205 and SW620) cells. It has been shown that mesenchymal matrix proteins such as fibronectin and collagen-I can induce taxol resistance in a 2D culture system by a β1-integrin mechanism that depends on Akt/PKB (Aoudjit and Vuori, 2001). Therefore, we tested whether the 3D matrix-induced changes in resistance or sensitivity to taxol treatment could be prevented or reversed in the presence of the β1-integrin function-blocking antibody mAb13 (Akiyama et al., 1989). In addition, to test whether the effects observed were dependent on the matrix configuration (3D matrix) versus the matrix composition (2D matrix), we tested the taxol responses in the presence or absence of β1-integrin inhibition using 2D plastic control as a contrasting substrate.

Our results show that β1-integrin blockade reversed the 3D matrix-induced taxol resistance in both PANC-1 and HS 578T cells, as well as the 3D matrix-induced sensitivity observed in PA-1 cells (Figure 6). β1-integrin blockade had no effect in COLO 205 and SW620 cells (Figure 6). While the observed response was specific to 3D matrix in PANC-1 and HS 578T cells, both 3D and 2D matrix induced a β1-integrin sensitivity in PA-1 cells that was independent from taxol responses (compare results in Figure 5J and Figure 6). These results suggest that conformation-dependent and conformation-independent responses to drug treatments vary from cell to cell, but that only cells that respond to matrix for control of growth or morphology have the tendency to also respond for drug treatments.

In parallel, lysates from this experiment were analyzed by Western blot with antibodies to two well-defined β1-integrin effectors, focal adhesion kinase (FAK) and Akt (Figure 7), as well as the important apoptotic regulator NF-κB (not shown). Total and activated (pFAK-Y^{397}) FAK and total and activated (pAkt-S^{473}) Akt were measured. As shown in Figure 7, mAb13 to β1-integrin specifically reduced the level of FAK activation in HS 578T, PANC-1 and SW620 cells grown in 3D matrices, while not affecting FAK activation in these cells grown in 2D. In contrast, little if any effect was seen with PA-1 and COLO 205 cells. These observations were compatible with the suggestion that 3D and 2D substrates differentially regulate integrins and their downstream effectors such as FAK (Paszek et al., 2005;Rhee et al., 2007;Wozniak et al., 2003). However, the fact the set of cells with 3D-regulated changed in FAK phosphorylation was different from those cells with 3D-regulated, integrin-dependent taxol resistance indicated an increased level of FAK activity could not explain this response.

PANC-1 cells grown in 3D matrices showed an increase in Akt activity, while no significant changes in Akt activity were observed in the other cell lines (Figure 7A). This again argued against a simple correlation of pathway activation with taxol response. Interestingly, on both 2D and 3D matrix, taxol treatment reduced the total expression levels of FAK and Akt (Figure 7), as well as of NFκB (not shown), while leaving the ratio of activated to total protein unchanged (Figure 7). However, comparison of relative FAK and Akt/PKB activity levels (see Methods) also suggested that for neither protein did activation status correlate with β1-integrin-dependent rescue (compare Figure 6 to Figure 7B and 7C). Similar results were observed with NFκB (not shown). These data suggest that although β1-integrin blockade effectively reversed the 3D matrix induced taxol responses (e.g., PANC-1, HS 578T and PA-1), the survival mechanism did not involve 3D matrix-induced activation of FAK, Akt/PKB, or NFκB.

Discussion

This study has several important implications for analysis of tumor cell growth and drug responses. First, using a novel fibroblast-derived 3D matrix system, we segregated tumor cell

lines into different classes based on the magnitude of their responsiveness to matrix and the degree to which matrix induces proliferative versus morphological changes in growth. The morphological responses we documented included increased acquisition of a spindle morphology by some cells, and rounded or amoeboid-like morphology by others. *In vivo*, as tumors become invasive, some neoplastic cells leave the tumor mass and undergo epithelial to mesenchymal transition (EMT), in which single cells (as opposed to tumor aggregates) assume a spindle shape or a mesenchymal fibroblast-like appearance. Conversely, metalloproteinase inhibitors, loss of p53, inhibition of the E3 ubiquitin ligase Smurf1, and other conditions which activate RhoA, trigger a mesenchymal to amoeboid transition (MAT), wherein tumor cells become rounded, thus modifying their survival and invasive behaviors (Condeelis and Segall, 2003; Gadea et al., 2007; Sahai et al., 2007; Sahai and Marshall, 2003). The 3D culture system we described here is well designed to analyze the behavior of isolated single cells that have undergone EMT or MAT and are invading through mesenchymal stroma.

As context, other recent studies have also explored 3D substrates as screening platforms to study tumor behavior. For example, Kenny and co-workers have analyzed spheroids, acini and cell aggregates, which mimic tumor masses that interact with basement membrane-like 3D substrates (Kenny et al., 2007). These 3D laminin gel-based cultures induced four distinct tumor-mass morphologies, specific to the 3D environment. Moreover, these cell-aggregate morphologies were each associated with specific gene expression profiles, which correlated with increased invasive tumor cell potential (Kenny et al., 2007). Together, platforms addressing single cell and aggregate cell growth in 3D have the potential to parse the different signaling conditions induced by tumor microenvironment.

We suggest that characterizing the morphological changes in isolated tumor cells on fibroblast-derived 3D matrices may allow rapid testing of how a specific tumor cell type will react to the microenvironment, thus facilitating the development of strategies for its specific treatment. For example, in our study PANC-1 adopts a rounded, amoeboid-like, morphology on 3D matrices. Amoeboid-like motility is not dependent on the activity of matrix metalloproteinases, but instead requires the action of RhoA GTPase (Friedl, 2004; Friedl and Wolf, 2003; Sahai and Marshall, 2003). This matrix-induced specific morphological behavior may predict that MMP inhibitors will not affect invasion of PANC-1 cells through tumor stroma, but that treatment of these cells with Rho inhibitors may successfully block their migration.

Second and importantly, our data suggest that the tendency of a cell to undergo morphological change (rounded or spindle) following plating onto stroma-like matrix may predict a tendency of matrix to influence drug response by that cell line (compare data with PANC-1, HS 578T and PA-1 versus COLO 205 and SW620). The profile of behavior of PA-1 indicates that the fact that 3D matrix can influence cell morphology does not predict whether change in drug response will be positive or negative; rather, this needs to be assessed for individual cell lines. Why 3D matrix induced response to taxol but not to other drugs remains to be determined. Nevertheless, it is intriguing that among those tested this agent alone targets the cytoskeleton. In this context, it has been reported that in breast cancer cells seeded onto isolated ECM proteins (e.g., fibronectin and type I collagen), β1-integrin is essential to developing resistance to taxol-induced apoptosis (Aoudjit and Vuori, 2001). It is also interesting to note that taxol has been reported to induce focal adhesion disorganization, with the associated taxol-dependent cell death rescued by integrin linked kinase (Deschesnes et al., 2007). Integrin overexpression frequently depresses levels of E-cadherin expression (Thiery and Sleeman, 2006); it has also been reported that loss of E-cadherin causes resistance to taxol (Ferreira et al., 2005). We hypothesize that a combination of specific ECM proteins, presented to tumor cells in association with a 3D architecture and β1-integrins, particularly enhances taxol responses by altering adhesion structure organization and signaling.

Other groups have also identified 3D matrix-dependent regulation of drug responses, using different culture systems. For example, Fischbach and colleagues used engineered polymeric scaffolds with carcinoma cells as 3D human tumor models, and have recently shown these synthetic matrices to effectively mimic many aspects of *in vivo* tumor behavior including some resistance to drugs (Fischbach et al., 2007). As another example, Weaver et. al. have demonstrated that Matrigel generates a β4-integrin-regulated cell polarization, which induces drug resistance in tumor cells derived from epithelial cells (Weaver et al., 2002). This significant study also showed that for some drugs, disrupting hemidesmosome formation perturbed matrix-directed tissue polarization, and subsequently inhibited NFκB activation, thus promoting apoptosis. We have also tested integrin-dependent NFκB activities in the presence of taxol using the 3D culture system described here. Our results indicate that although NFκB activity was induced by 3D fibroblast matrix, these changes were not reversed by integrin inhibition (data not shown), indicating activation of NFκB does not influence drug resistance in this system.

We propose that a 3D matrix system prepared from stable cell lines such as NIH3T3 can provide a convenient and highly physiological assay system to measure and correlate cell morphology, proliferation, tendency to apoptosis, and drug response in high throughput formats. Further, we have recently described a “progressive” stromal system in which we compared the properties of 3D matrices prepared from normal, carcinogen-primed, and tumor-associated fibroblasts (Amatangelo et al., 2005; Castelló-Cros and Cukierman, 2008). The data presented in the present study indicate that most of the cell lines evaluated proliferated better on plastic or 2D matrix substrates than on the *in vivo*-like 3D matrix. Notably, the 3D matrix used in this study represents an early stromagenic stage in tumor development, which may still impose the restrictive natural barrier of the host’s stroma (Amatangelo et al., 2005). Based on the results described here, it is likely that these staged, progressive matrices will each differentially interact with tumor cell lines, allowing further parsing of the tumor-microenvironment dialog. We believe that in the future, specific fibroblast-derived matrices representing different stages of tumor progression, from different tumor types, would enhance the screening for drug response in discrete classes of tumor cell lines, i.e. pairing tumor-associated fibroblast-derived 3D matrices with tissue-specific neoplastic cells should better predict matrix-induced drug responses for the cancer in question (e.g., breast or pancreas). Carefully selecting cells, drugs and microenvironmental settings is important, as many drugs that are potent in *in vitro* biochemical assays and/or in conventional assays performed on cultured cells fail at the stage of *in vivo* assays tested in animals. Extended work in this area may help develop more robust *in vitro* drug screening regimens that will better mimic *in vivo* settings, thus reducing the failure rate of drug leads in pre-clinical development.

Experimental Procedures

Cell lines and antibodies

The 11 cancer cell lines were from the NCI panel of 60 cancer cell lines (Stinson et al., 1992); HS 578T and PANC-1 were a gift from Dr. Vladimir Khazaksome, PA-1; PA-1/E6 (Wu and El-Deiry, 1996); HCT116/p53- (Bunz et al., 1998) were from Dr. Maureen Murphy and the rest were purchased from ATCC. Culturing conditions for each cell line were as suggested by ATCC. Monoclonal anti-Akt antibody was obtained from BD Bioscience (San Jose, CA) and polyclonal rabbit anti-pAkt-S^{473} antibody was from Cell Signaling (Beverly, MA). Monoclonal anti-GADPH (Chemicon Int, Millipore), FAK (Upstate, Millipore), pFAK-Y^{397} was from Biosource international (Camarillo, CA). IRDye800-labeled goat anti-rabbit antibody, IRDye680-labeled goat anti-mouse antibody, Odyssey blocking buffer and infrared Odyssey scanner and were obtained from LI-COR (Lincoln, NE). StartingBlock™ T20 (TBS) Blocking Buffer was purchased from Pierce (Rockford, IL). Functional blocking anti β1-

integrin antibody, mAb13 (Akiyama et al., 1989), was kindly provided by Kenneth M. Yamada (NIH/NIDCR/CDBRB, Bethesda MD). Purified Rat IgG used as non-specific antibody control was from Sigma Aldrich.

Production of Fibroblast-derived 3D Matrix

NIH3T3 cells were cultured in maintenance medium (high glucose Dulbecco's Modified Eagle's Medium containing 10% fetal bovine serum (FBS), 100 units/ml penicillin and 100 μg/ml streptomycin) for a minimum of 20 passages prior to matrix production, to overcome their normal contact growth inhibition (Beacham et al., 2006; Cukierman, 2002; Cukierman, 2005). To prepare matrix for use, confluent NIH3T3 cultures were treated with fresh maintenance media supplemented with 50 μg/ml cell culture-tested ascorbic acid (Sigma-Aldrich, St. Louis, MO) every other day for 8 days, based on previously established protocols (Cukierman, 2002; Cukierman, 2005). After eight days of ascorbic acid treatment, all cultures were examined under the microscope for quality control. Alkaline detergent treatment (0.5% (v/v) Triton ×-100 and 20 mM NH_4OH) of these cultures, followed by PBS washing (3x), yielded cell-free *in vivo*-like 3D matrices that remained attached to the culture plates. The resulting extracted 3D matrices were stored at 4°C in PBS containing 100 units/ml penicillin and 100 μg/ml streptomycin until needed. Cells from a panel of epithelial cancer cell lines (see Table 1) were seeded onto these extracted 3D matrices for all experiments presented herein.

Assessment of Cancer Cell Growth

Numbers of living cells were evaluated with the nontoxic dye Alamar Blue (Invitrogen), according to the manufacturer's protocol. Briefly, cell lines were plated at a density of 2000 cells/well in 96 well plates (or 10,000 cell/well in 48 well plates) directly onto tissue culture plastic, NIH3T3-derived 3D matrix, or tissue culture plastic pre-coated with 6M guanidine-solubilized NIH3T3-derived 2D matrix mix (prepared as in (Beacham et al., 2006; Cukierman, 2002; Cukierman, 2005)). Cells were grown for 24h, 48h or 72h and then treated with 10% (v/v) Alamar Blue solution. The cells were incubated for 4h in the presence of dye, then changes in fluorescence ratio were measured at 535/595 using a SpectraFluor Plus (Tecan) fluorecent platereader. For each condition, wells without cells but containing culture medium and Alamar Blue were used as negative control. All assays were performed a minimum of three times and conditions were tested in triplicate.

Drug treatment and IC50 determination

Cells were seeded into 96 well plates on tissue culture plastic or NIH3T3 cell-derived 3D matrix. After 24h, concentrations of drugs indicated in Results prepared in 10% PBS-medium (Gleevec) or in 10% DMSO-medium (Taxol, MCP-1, Gefitinib and Sorafenib) were added. Vehicles were used as controls. At day three (48 hours after drug addition), 10% (v/v) Alamar Blue was added to each well. Fluorescence was measured for growth determination. IC50 values were obtained using Excelfit software. Experimental conditions were set so that drug-induced cell killing was between 15% and 85% of untreated control cells, on 2D control conditions. All experiments were performed in triplicate, with three independent experiments for each result reported. During experiments testing β1-integrin blockage, mAb13 was used at a final concentration of 50μg/ml and taxol was used at 10nM for COLO 205 and HS 578T, 100nM for PANC-1, 20nM for PA-1 and 25nM for SW620. Negative controls included non-specific rat IgG at final concentration of 50μg/ml and/or 1% DMSO (see Western blot for statistics).

Drug Induced Apoptosis. To measure apoptosis, a kit-based assay employing the APOP*ercentage* Dye (Biocolor, Co, UK) was used, according to manufacturer's instructions. Briefly, cells were plated on 96 well plates on tissue culture plastic or onto 3D matrix. After 24 hours, indicated concentrations of the drugs or vehicle controls were added, then cells

incubated an additional 48h. Cells were then labeled in parallel with APOP*ercentage* Dye diluted 1:20 to detect apoptotic cells and with 0.5 μM Calcein AM (Invitrogen) to detect viable cells. Cells were labeled for a period of 30 min at 37°C, and rinsed twice with PBS. Fluorescent dual channeled images were obtained from a mercury light source using excitation 530–560 and 465–495 and emission 573–648 and 515–555 filters for APOP*ercentage* (red) and Calcein AM (green), respectively. The images were acquired with a 10X objective on an inverted Nikon Eclipse TE2000-U microscope. The relative rate of apoptosis was calculated utilizing digital analyses obtained from MetaMorph 7.0.4; the percentage shown corresponds to total count (viable plus apoptotic cell areas) divided by apoptotic cell areas.

Western blot

A total of 1×10^5 cells were plated for 24h onto each well of plastic control or fibroblast-derived 3D matrix coated 6-well plates. The following day, indicated concentrations of mAb13, taxol or vehicles, used as control, were added. After 48h of incubation, the cells were lysed using a modified RIPA buffer lacking sodium dodecyl sulfate, consisting of 50 mmol/L Tris pH 8.0, 150 mmol/L NaCl, 5 mmol/L benzamidine, 10% glycerol, 48 mmol/L NaF, 1% deoxycholate salt (w/v), 1% Triton X-100, 1 mmol/L sodium pyrophosphate, 1 mmol/L nitrophenol phosphate, 1 mmol/L phenylmethyl sulfonyl fluoride, 1 mmol/L sodium orthovanadate, and mammalian protease inhibitor cocktail (Sigma-Aldrich). Cell lysates were separated by sodium dodecyl sulfate-polyacrylamide gel electrophoresis using precast Tris-glycine 8 to 16% gels (Invitrogen). The proteins were then transferred to polyvinylidene difluoride membranes (Millipore) following manufacturer's instructions. Membranes were incubated for 1h in Odyssey blocking buffer and incubated overnight at 4°C with assorted primary antibodies (GADPH 1:5000, Akt (1:2000), phospo-Akt (1:1000), FAK (1:2000) and phospho-FAK (1:2000)) diluted in StartingBlock™ T20 (TBS) Blocking Buffer. Next day, the antibody solution was discarded and the membranes were washed four times for 5 min each with 0.1% Tween 20/PBS. Then, the membranes were incubated for 1h at room temperature with the secondary solution containing IRDye800-labeled goat anti-rabbit antibody, IRDye680-labeled goat anti-mouse antibody diluted at 1:15.000 in StartingBlock™ T20 (TBS) Blocking Buffer. After washing four times with 0.1% Tween 20/PBS, the membrane was rinsed once with PBS and scanned by the Odyssey infrared scanner. The optical densities of protein bands were quantified using the scanner's software. For statistics, we calculated the standard errors of the log ratio ((2D:3D)taxol/mAb13) using the multivariate delta method (Beyene and Moineddin, 2005), and used a Wald test to assess statistical significance.

Supplementary Material

Refer to Web version on PubMed Central for supplementary material.

Acknowledgments

We thank Drs. Maureen Murphy, Gary Kruh, Vladimir Khazak, and Margret Einarson (of the Fox Chase Cancer Center Translational Facility) for contributing cell lines and drugs to this study, Dr. Brian Egleston (of the Fox Chase Cancer Center Biostatistics and Bioinformatics Facility) for statistical analyses, Dr. Jonathan Cheng, for critical comments and K. Buchheit for assertive proofreading. This work was supported by the following: the American Association of Cancer Research (the department specifically disclaims responsibility for any analyses, interpretations, or conclusions), the WW Smith charitable trust, the Erwin Trust in support for pancreatic cancer the Ovarian Cancer Research Fund, as well as, NIH/NCI Ovarian Cancer SPORE (P50 CA083638), core grant (CA-06927), RO1 CA113451 (to EC), and RO1 CA63366 (to EG), and an appropriation from the Commonwealth of Pennsylvania.

References

Akashi T, Minami J, Ishige Y, Eishi Y, Takizawa T, Koike M, Yanagishita M. Basement membrane matrix modifies cytokine interactions between lung cancer cells and fibroblasts. Pathobiology 2005;72:250–259. [PubMed: 16374069]

Akiyama SK, Yamada SS, Chen WT, Yamada KM. Analysis of fibronectin receptor function with monoclonal antibodies: roles in cell adhesion, migration, matrix assembly, and cytoskeletal organization. J Cell Biol 1989;109:863–875. [PubMed: 2527241]

Amatangelo MD, Bassi DE, Klein-Szanto AJ, Cukierman E. Stroma-derived three-dimensional matrices are necessary and sufficient to promote desmoplastic differentiation of normal fibroblasts. Am J Pathol 2005;167:475–488. [PubMed: 16049333]

Amenta PS, Hadad S, Lee MT, Barnard N, Li D, Myers JC. Loss of types XV and XIX collagen precedes basement membrane invasion in ductal carcinoma of the female breast. J Pathol 2003;199:298–308. [PubMed: 12579531]

Aoudjit F, Vuori K. Integrin signaling inhibits paclitaxel-induced apoptosis in breast cancer cells. Oncogene 2001;20:4995–5004. [PubMed: 11526484]

Beacham, DA.; Amatangelo, MD.; Cukierman, E. Preparation of Extracellular Matrices Produced by Cultured and Primary Fibroblasts. In: Bonifacino, JS.; Dasso, M.; Lippincott-Schwartz, J.; Harford, JB.; Yamada, KM., editors. Curr Protocols Cell Biol. John K. Wiley & Sons; 2006. p. 10.09.01-10.09.21.

Beyene J, Moineddin R. Methods for confidence interval estimation of a ratio parameter with application to location quotients. BMC Med Res Methodol 2005;5:32. [PubMed: 16221306]

Bhowmick NA, Neilson EG, Moses HL. Stromal fibroblasts in cancer initiation and progression. Nature 2004;432:332–337. [PubMed: 15549095]

Bissell MJ, Labarge MA. Context, tissue plasticity, and cancer: are tumor stem cells also regulated by the microenvironment? Cancer Cell 2005;7:17–23. [PubMed: 15652746]

Bissell MJ, Radisky DC, Rizki A, Weaver VM, Petersen OW. The organizing principle: microenvironmental influences in the normal and malignant breast. Differentiation 2002;70:537–546. [PubMed: 12492495]

Bunz F, Dutriaux A, Lengauer C, Waldman T, Zhou S, Brown JP, Sedivy JM, Kinzler KW, Vogelstein B. Requirement for p53 and p21 to sustain G2 arrest after DNA damage. Science 1998;282:1497–1501. [PubMed: 9822382]

Capo-Chichi CD, Smith ER, Yang DH, Roland IH, Vanderveer L, Cohen C, Hamilton TC, Godwin AK, Xu XX. Dynamic alterations of the extracellular environment of ovarian surface epithelial cells in premalignant transformation, tumorigenicity, and metastasis. Cancer 2002;95:1802–1815. [PubMed: 12365030]

Castelló-Cros, R.; Cukierman, E. Stromagenesis during tumorigenesis: characterization of tumor-associated fibroblasts and stroma-derived 3D matrices. In: Even-Ram, S., editor. Methods Mol. Biol. Totowa, NJ: Humana Press; 2008. in press

Chaponnier C, Gabbiani G. Pathological situations characterized by altered actin isoform expression. J Pathol 2004;204:386–395. [PubMed: 15495226]

Condeelis J, Segall JE. Intravital imaging of cell movement in tumours. Nat Rev Cancer 2003;3:921–930. [PubMed: 14737122]

Cukierman, E. Preparation of Extracellular Matrices Produced by Cultured Fibroblasts. In: Bonifacino, JS.; Dasso, M.; Lippincott-Schwartz, J.; Harford, JB.; Yamada, KM., editors. Curr Protocols Cell Biol. John K. Wiley & Sons; 2002. p. 10.09.01-10.09.14.

Cukierman, E. Cell migration analyses within fibroblast-derived 3-D matrices. In: Guan, J., editor. Cell migration: Developmental methods and protocols. Totowa, NJ: Humana Press; 2005. p. 79-93.

Cukierman E, Pankov R, Stevens DR, Yamada KM. Taking cell-matrix adhesions to the third dimension. Science 2001;294:1708–1712. [PubMed: 11721053]

Cukierman E, Pankov R, Yamada KM. Cell interactions with three-dimensional matrices. Curr Opin Cell Biol 2002;14:633–640. [PubMed: 12231360]

Damianova R, Stefanova N, Cukierman E, Momchilova A, Pankov R. Three-dimensional matrix induces sustained activation of ERK1/2 via Src/Ras/Raf signaling pathway. Cell Biol Int. 2007in press

Deschesnes RG, Patenaude A, Rousseau JL, Fortin JS, Ricard C, Cote MF, Huot J, R CG, Petitclerc E. Microtubule-destabilizing agents induce focal adhesion structure disorganization and anoikis in cancer cells. J Pharmacol Exp Ther 2007;320:853–864. [PubMed: 17099073]

Desmouliere A, Guyot C, Gabbiani G. The stroma reaction myofibroblast: a key player in the control of tumor cell behavior. Int J Dev Biol 2004;48:509–517. [PubMed: 15349825]

Ferreira P, Oliveira MJ, Beraldi E, Mateus AR, Nakajima T, Gleave M, Yokota J, Carneiro F, Huntsman D, Seruca R, Suriano G. Loss of functional E-cadherin renders cells more resistant to the apoptotic agent taxol in vitro. Exp Cell Res 2005;310:99–104. [PubMed: 16112667]

Fischbach C, Chen R, Matsumoto T, Schmelzle T, Brugge JS, Polverini PJ, Mooney DJ. Engineering tumors with 3D scaffolds. Nat Methods 2007;4:855–860. [PubMed: 17767164]

Frankel A, Buckman R, Kerbel RS. Abrogation of taxol-induced G2-M arrest and apoptosis in human ovarian cancer cells grown as multicellular tumor spheroids. Cancer Res 1997;57:2388–2393. [PubMed: 9192815]

Friedl P. Prespecification and plasticity: shifting mechanisms of cell migration. Curr Opin Cell Biol 2004;16:14–23. [PubMed: 15037300]

Friedl P, Wolf K. Tumour-cell invasion and migration: diversity and escape mechanisms. Nat Rev Cancer 2003;3:362–374. [PubMed: 12724734]

Gadea G, de Toledo M, Anguille C, Roux P. Loss of p53 promotes RhoA-ROCK-dependent cell migration and invasion in 3D matrices. J Cell Biol 2007;178:23–30. [PubMed: 17606864]

Griffith LG, Swartz MA. Capturing complex 3D tissue physiology in vitro. Nat Rev Mol Cell Biol 2006;7:211–224. [PubMed: 16496023]

Grinnell FB, Rocha L, Iucu C, Rhee S, Jiang H. Nested collagen matrices: A new model to study migration of human fibroblast populations in three dimensions. Experimental Cell Research 2006;312:86–94. [PubMed: 16256985]

Grinnell F, Fukamizu H, Pawelek P, Nakagawa S. Collagen processing, crosslinking, and fibril bundle assembly in matrix produced by fibroblasts in long-term cultures supplemented with ascorbic acid. Exp Cell Res 1989;181:483–491. [PubMed: 2924799]

Hazlehurst LA, Landowski TH, Dalton WS. Role of the tumor microenvironment in mediating de novo resistance to drugs and physiological mediators of cell death. Oncogene 2003;22:7396–7402. [PubMed: 14576847]

Hwang NS, Kim MS, Sampattavanich S, Baek JH, Zhang Z, Elisseeff J. Effects of three-dimensional culture and growth factors on the chondrogenic differentiation of murine embryonic stem cells. Stem Cells 2006;24:284–291. [PubMed: 16109760]

Kenny PA, Lee GY, Myers CA, Neve RM, Semeiks JR, Spellman PT, Lorenz K, Lee EH, Barcellos-Hoff MH, Petersen OW, et al. The morphologies of breast cancer cell lines in three-dimensional assays correlate with their profiles of gene expression. Molecular Oncology 2007;1:84–96. [PubMed: 18516279]

Kim JB. Three-dimensional tissue culture models in cancer biology. Seminars in Cancer Biology 2005;15:365–377. [PubMed: 15975824]

Kleinman HK, Martin GR. Matrigel: Basement membrane matrix with biological activity. Sem Can Biol 2005;15:378–386.

Kleinman HK, McGarvey ML, Hassell JR, Star VL, Cannon FB, Laurie GW, Martin GR. Basement membrane complexes with biological activity. Biochemistry 1986;25:312–318. [PubMed: 2937447]

Mareel M, Leroy A. Clinical, cellular, and molecular aspects of cancer invasion. Physiol Rev 2003;83:337–376. [PubMed: 12663862]

Morin PJ. Drug resistance and the microenvironment: nature and nurture. Drug Resistance Updates 2003;6:169–172. [PubMed: 12962682]

Muller U. Integrins and extracellular matrix in animal models. Cell Adhesion 2004:217–241.

Netto MV, Mohan RR, Sinha S, Sharma A, Dupps W, Wilson SE. Stromal haze, myofibroblasts, and surface irregularity after PRK. Exp Eye Res 2006;82:788–797. [PubMed: 16303127]

Pankov R, Endo Y, Even-Ram S, Araki M, Clark K, Cukierman E, Matsumoto K, Yamada KM. A Rac switch regulates random versus directionally persistent cell migration. J Cell Biol 2005;170:793–802. [PubMed: 16129786]

Park CC, Bissell MJ, Barcellos-Hoff MH. The influence of the microenvironment on the malignant phenotype. Mol Med Today 2000;6:324–329. [PubMed: 10904250]

Paszek MJ, Zahir N, Johnson KR, Lakins JN, Rozenberg GI, Gefen A, Reinhart-King CA, Margulies SS, Dembo M, Boettiger D, et al. Tensional homeostasis and the malignant phenotype. Cancer Cell 2005;8:241–254. [PubMed: 16169468]

Rhee S, Jiang H, Ho CH, Grinnell F. Microtubule function in fibroblast spreading is modulated according to the tension state of cell-matrix interactions. Proc Natl Acad Sci U S A 2007;104:5425–3540. [PubMed: 17369366]

Sahai E, Garcia-Medina R, Pouyssegur J, Vial E. Smurf1 regulates tumor cell plasticity and motility through degradation of RhoA leading to localized inhibition of contractility. J Cell Biol 2007;176:35–42. [PubMed: 17190792]

Sahai E, Marshall CJ. Differing modes of tumour cell invasion have distinct requirements for Rho/ROCK signalling and extracellular proteolysis. Nat Cell Biol 2003;5:711–719. [PubMed: 12844144]

Soto AM, Sonnenschein C. Emergentism as a default: Cancer as a problem of tissue organization. J Biosci 2005;30:103–118. [PubMed: 15824446]

Stinson SF, Alley MC, Kopp WC, Fiebig HH, Mullendore LA, Pittman AF, Kenney S, Keller J, Boyd MR. Morphological and immunocytochemical characteristics of human tumor cell lines for use in a disease-oriented anticancer drug screen. Anticancer Res 1992;12:1035–1053. [PubMed: 1503399]

Thiery JP, Sleeman JP. Complex networks orchestrate epithelial-mesenchymal transitions. Nat Rev Mol Cell Biol 2006;7:131–142. [PubMed: 16493418]

Weaver VM, Lelievre S, Lakins JN, Chrenek MA, Jones JC, Giancotti F, Werb Z, Bissell MJ. beta4 integrin-dependent formation of polarized three-dimensional architecture confers resistance to apoptosis in normal and malignant mammary epithelium. Cancer Cell 2002;2:205–216. [PubMed: 12242153]

Wozniak MA, Desai R, Solski PA, Der CJ, Keely PJ. ROCK-generated contractility regulates breast epithelial cell differentiation in response to the physical properties of a three-dimensional collagen matrix. J Cell Biol 2003;163:583–595. [PubMed: 14610060]

Wu GS, El-Deiry WS. p53 and chemosensitivity. Nat Med 1996;2:255–256. [PubMed: 8612210]

Yamada KM, Cukierman E. Modeling tissue morphogenesis and cancer in 3D. Cell 2007;130:601–610. [PubMed: 17719539]

Yang WL, Godwin AK, Xu XX. Tumor necrosis factor-alpha-induced matrix proteolytic enzyme production and basement membrane remodeling by human ovarian surface epithelial cells: molecular basis linking ovulation and cancer risk. Cancer Res 2004;64:1534–1540. [PubMed: 14973065]

Zahir N, Weaver VM. Death in the third dimension: apoptosis regulation and tissue architecture. Curr Opin Genet Dev 2004;14:71–80. [PubMed: 15108808]

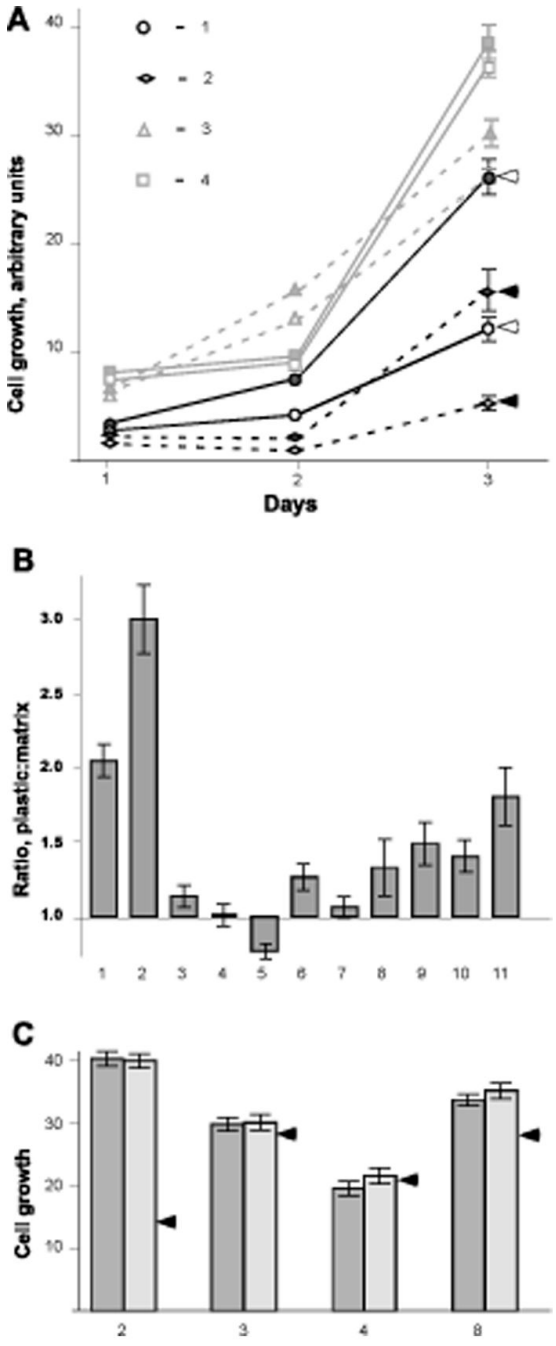

Figure 1. Growth on fibroblast-derived 3D matrix differentially regulates proliferation of a panel of human cancer cell lines

A. Growth of cell lines for 3 days following plating at a density of 2000 cells/well on NIH3T3 cell-derived 3D matrix or tissue culture plastic, prepared as in (Cukierman, 2002; Cukierman, 2005). Assays were run in 96 well plates. Conditions were tested in triplicate, and experiments were repeated three times independently. Results of one typical experiment are shown. Cell numbers were measured by Alamar Blue assay (Invitrogen) following manufacturer's instructions. Squares indicate COLO 205; triangles, PA-1; circles, HCT116; diamonds, NCI-H460 cells. Filled icons indicate cells grown on plastic while open icons indicate cells grown onto 3D matrix. Arrows designate cell lines with proliferation significantly influenced by

growth on 3D matrix. **B**. The relative proliferation ratio of cells on 3D matrix versus tissue culture plastic at day three after plating is shown. Ratios were calculated as (proliferation rate on plastic) / (proliferation rate onto matrix) as determined by Alamar Blue assay, and expressed in arbitrary units with background subtracted. On average, 4 experiments were performed for each cell line, with each cell line assessed in triplicate in each experiment. Cells shown are: 1, HCT116; 2, NCI-H460; 3, PA-1; 4, COLO 205; 5, PANC-1; 6, MCF7; 7, SW620; 8, HCT116/p53-; 9, HS 578T; 10, PA-1/E6; and 11, MCF10A. **C**. Relative proliferation of selected cell lines plated on 2D uncoated plastic (dark bars) versus onto plastic pre-coated with solubilized NIH3T3-derived matrix (light bars), to produce 2D matrix conditions as described in (Beacham et al., 2006; Cukierman, 2002; Cukierman et al., 2001). The arrows represent the relative level of proliferation for the given cell line on 3D matrix. Note that these values were extrapolated from the ratios observed in **B** and are shown with the purpose of comparing the two 2D conditions to the 3D matrix values. Numbers correspond to cell lines as in **B**.

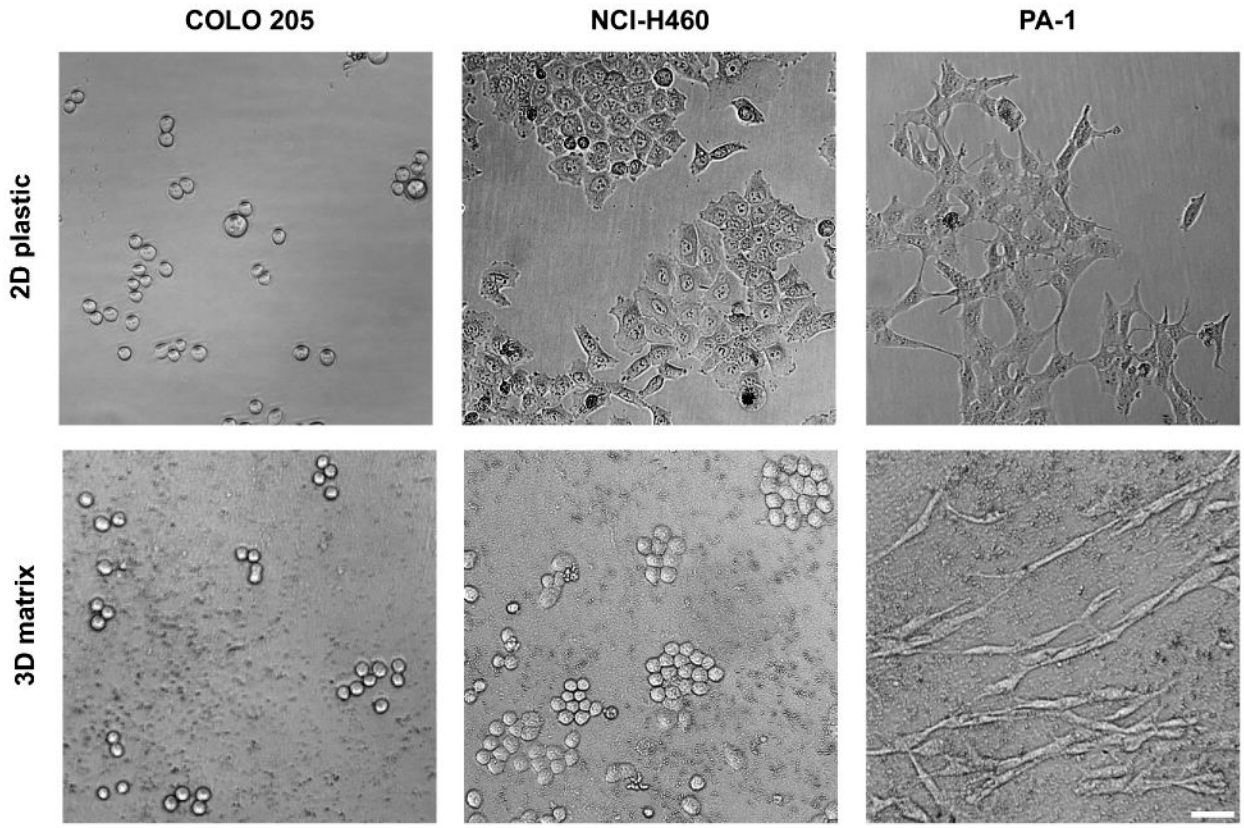

Figure 2. Growth on fibroblast-derived 3D matrix differentially regulates the morphology of human cancer cell lines

Cells were plated as in Figure 1A, and images acquired daily for 3 days. Images shown correspond to the second day on 3D matrix or on tissue culture 2D plastic (see supplemental Figure 1 for additional cell examples). Transmitted light phase contrast images were acquired using a 10X objective on an inverted Nikon Eclipse TE2000-U microscope. Scale bar, 50 μm.

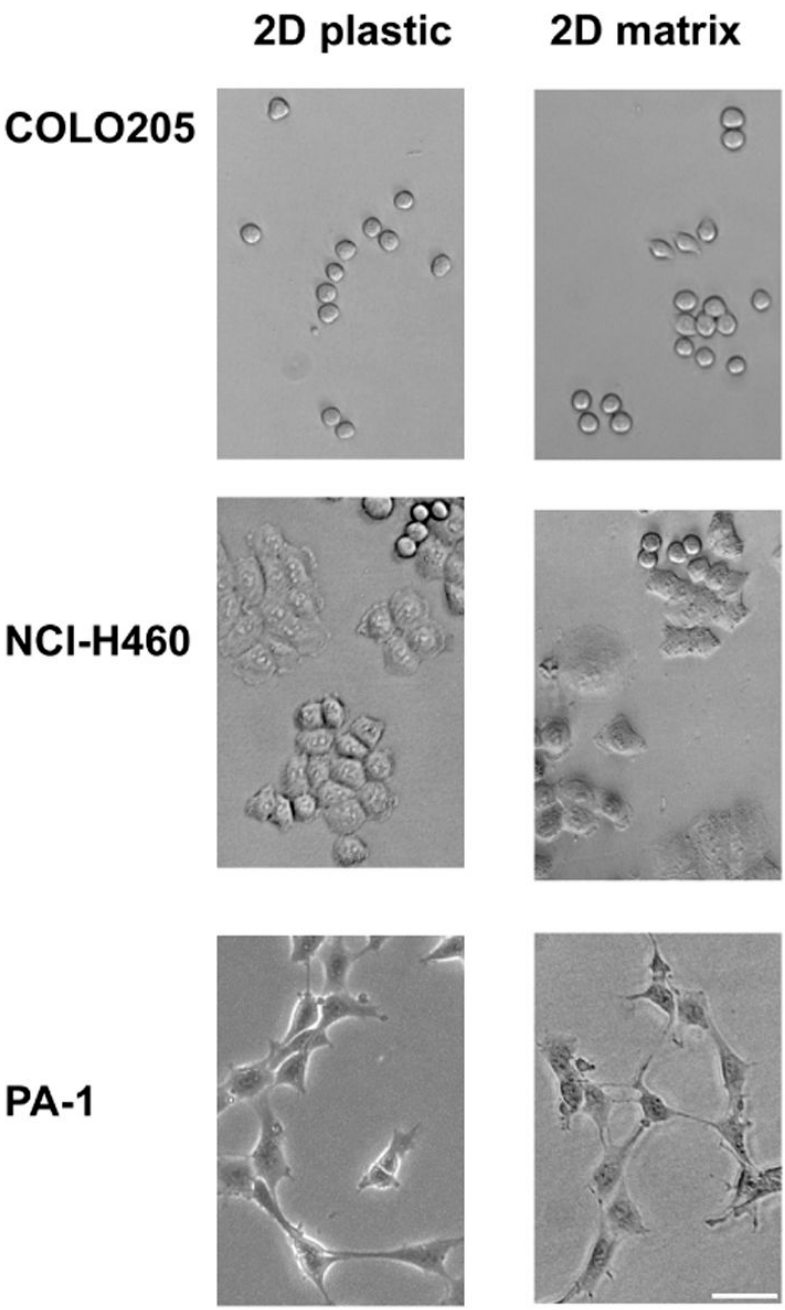

Figure 3. Solubilized 2D matrix does not induce morphological changes to assorted epithelial cancer cells

The indicated cell lines were comparatively grown on 2D NIH3T3 cell-derived matrix mix (Cukierman, 2002; Cukierman et al., 2001) or tissue culture plastic for 2 days. Images were acquired as indicated in Figure 2. Scale bar, 50 μm. Note that no differences in cell morphology were observed when culturing cells onto these 2D matrix substrate controls.

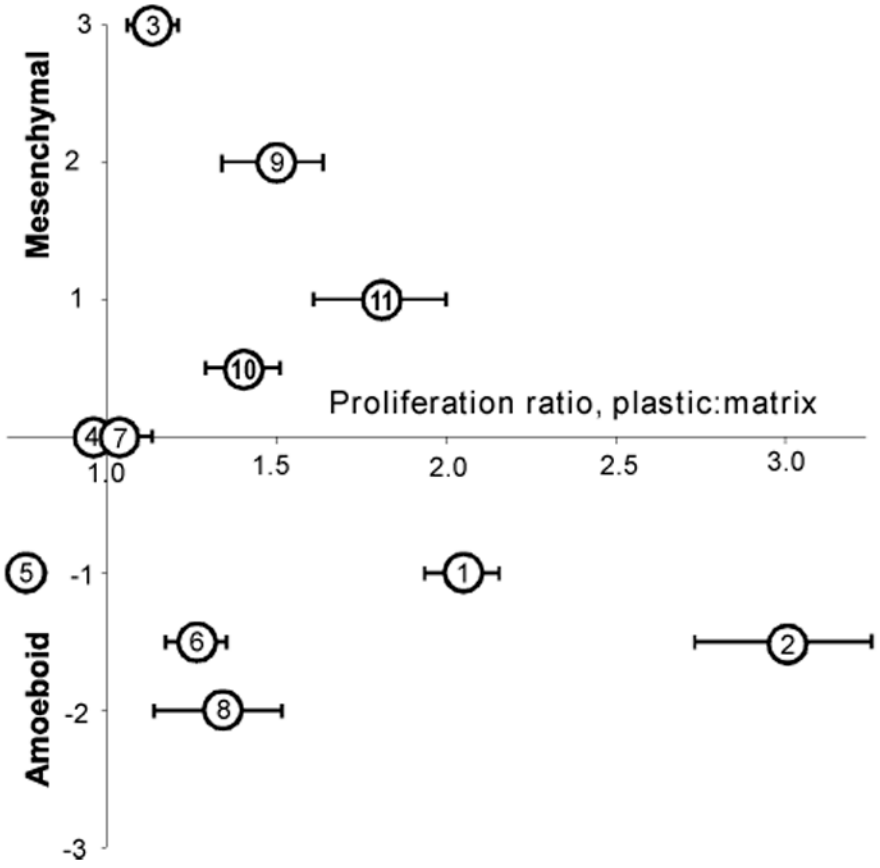

Figure 4. Epithelial cancer cell proliferative and morphological responses vary independently

Merged profiles of the proliferative and morphological responses to the matrix were plotted and are shown. Cell shown correspond to 1, HCT116; 2, NCI-H460; 3, PA-1; 4, COLO 205; 5, PANC-1; 6, MCF7; 7, SW620; 8, HCT116/p53-; 9, HS 578T; 10, PA-1/E6; and 11, MCF10A. Values were given arbitrary ranging from 0 for nonresponsive to 3 for very responsive cell.

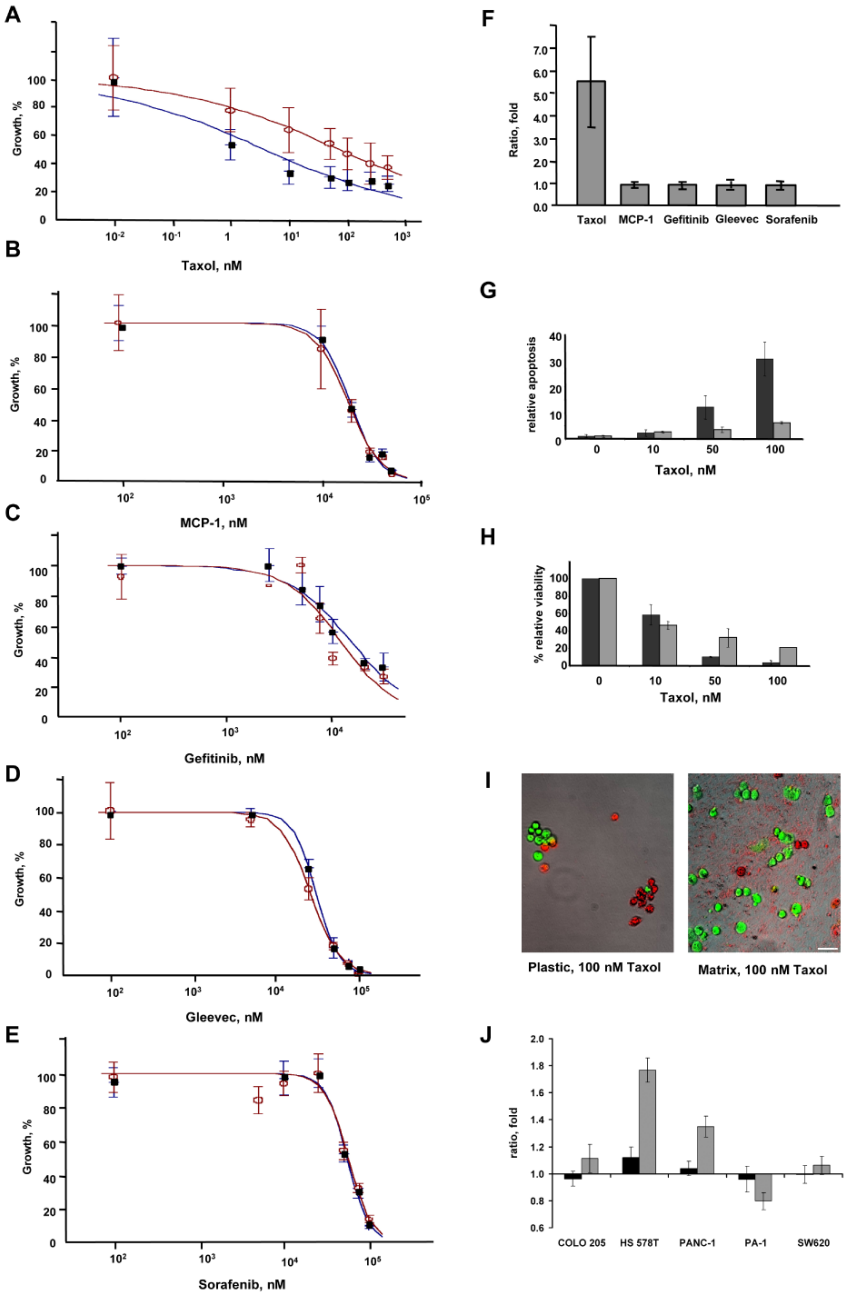

Figure 5. Fibroblast-derived 3D matrix selectively regulates human cancer cell responses to drugs

PANC-1 cells were grown on 3D matrix (open circles) or tissue culture plastic (closed circles), and treated with drugs at the concentrations indicated. IC50 calculation was done using Excelfit software. Drugs assessed included **A**, Taxol **B**, MCP-1, **C**, Gefitinib, **D**, Gleevec, and **E**, Sorafenib. **F**. Ratios of IC50 values (matrix:plastic) for PANC-1 cells grown on 3D matrix versus on plastic, 3 days after treatment with drugs are indicated. Results of three separate experiments performed in triplicate are shown. **G, H**. Apoptosis (**G**) and total cell number (**H**) were measured simultaneously on plastic (dark bars) or onto 3D matrix (light bars) using the APOPercentage kit (Biocolor, Co, UK) in conjunction with 0.5 Calcein AM to score total cell numbers (following the manufacturer's indications, Invitrogen). The relative rate of

apoptosis was calculated utilizing digital analyses obtained from MetaMorph 6.3; the percentage shown corresponds to total count (viable plus apoptotic cell areas; shown as green and red in **I** below) divided by apoptotic cell areas (red in **I**). **I**. Representative images of PANC-1 cells grown in the presence of 100 nM taxol for 3 days. Green indicates Calcein AM metabolic cell staining, while red indicates apoptotic cell areas obtained from APOPercentage dye staining. Images shown are a result of merging both fluorescent color channels and the corresponding transmitted phase contrast. Scale bar, 50 μm. **J**. Ratios of 2D matrix:plastic (dark bars) or 3D matrix:plastic (light bars) IC50 values for PANC-1, HS 578T, COLO 205, PA-1 and SW620 cells, three days after treatment with taxol. Results of three separate experiments performed in triplicate are shown.

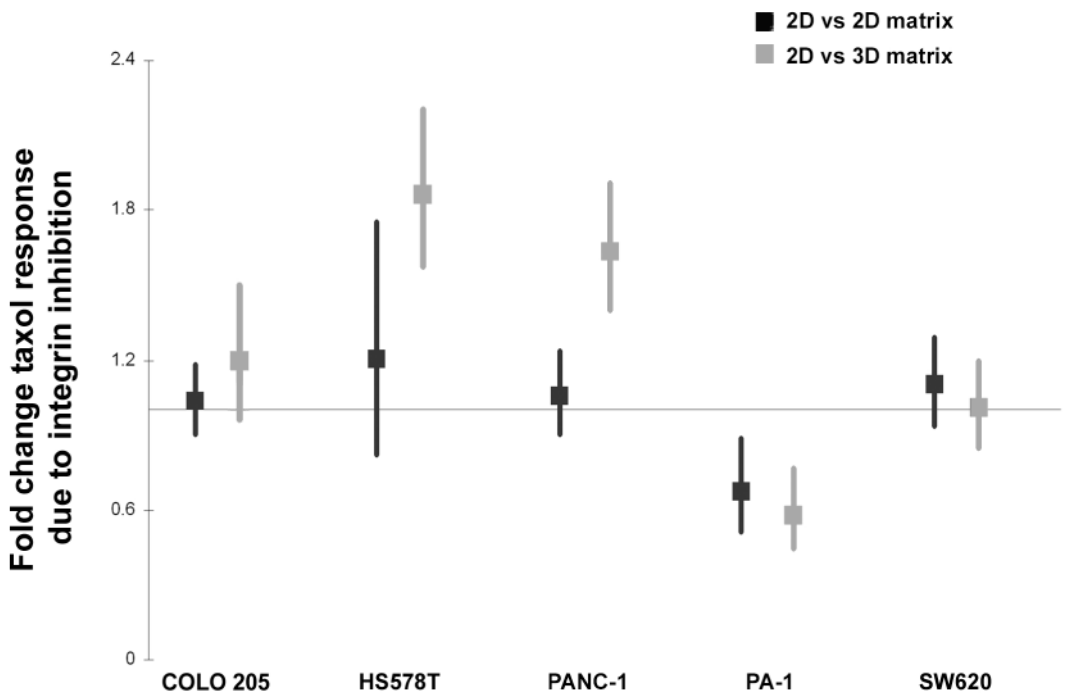

Figure 6. Fibroblast-derived 3D matrix selectively regulates human cancer cell resistance to taxol via β1-integrin activity

The cell lines indicated were cultured onto fibroblast-derived 3D matrices, or on 2D matrices or plastic as negative controls, in the presence or absence of taxol, β1-integrin functional blocking antibody mAb13 or a combination of both taxol and mAb13. Samples were tested for their viability using an Alamar blue assay. The ability of mAb13 to reverse the 2D (dark squares) or 3D matrix (light squares) induced resistance to taxol treatment was measured by the following log ratio ((plastic:matrix)taxol/mAb13) using the multivariate delta method, and the Wald test to assess statistical significance. In the graph, point estimates and associated 95% confidence intervals constructed using the standard error of the log ratio estimate are shown. Note that samples depicting point estimates larger or smaller than one, represent matrix induced resistance, which was effectively reversed by β1-integrin functional block. Log ratio points with error bars that do not cross the line are considered significant. Finally, a non-specific (Rat IGg) antibody, used as negative control, did not block the 3D matrix-induced responses observed to taxol treatment (not shown).

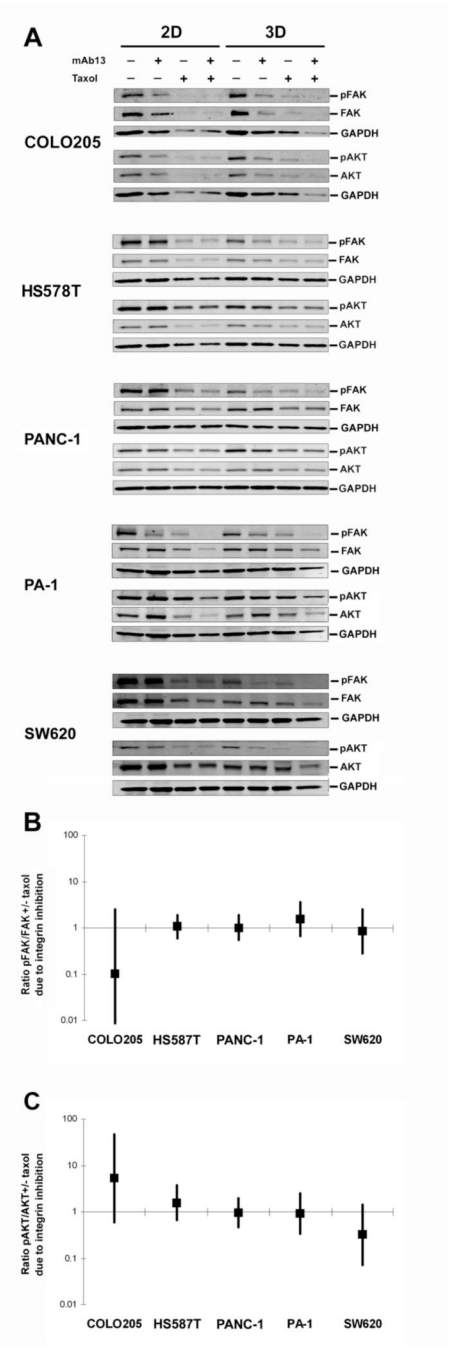

Figure 7. Fibroblast-derived 3D matrix responses to taxol are independent from FAK and Akt pathways

Cells were cultured on control 2D plastic or onto fibroblast-derived 3D matrices in the presence or absence of taxol, β1-integrin functional blocking antibody mAb13, or a combination of both taxol and mAb13. **A**. Representative Western blot analyses of total FAK or Akt and activated pFAK-Y^{397} (pFAK) and pAkt-S^{473} (pAkt). GAPDH served as loading control. **B**, **C**. The ability of mAb13 to reverse the matrixinduced responses to taxol through FAK (**B**) or Akt (**C**) activities, were expressed as the log ratio ((plastic:matrix)taxol/mAb13) using the multivariate delta method, and the Wald test to assess statistical significance, in analysis of three independent Western blots of experiments performed in triplicate. In the graphs (**B** and

C), point estimates and associated 95% confidence intervals constructed using the standard error of the log ratio estimate. Log ratio points with error bars that cross the line depicting a ratio that is equal to one are insignificant.

Table 1

Summary of epithelial cell lines and drugs used for analysis

This table lists the 11 human epithelial cancer cell lines used in this study, together with American Type Culture Collection identifying numbers (where available). Numbers for each line correspond to the numbers used throughout the manuscript. Drugs used in the study are shown and short descriptions of their targets are provided.

	Cell Line	Characteristics
1	HCT116	Human colorectal carcinoma; ATCC CCL-247
2	NCI-H460	Human large cell lung carcinoma; ATCC HTB-177
3	PA-1	Human ovarian teratocarcinoma; ATCC CRL-1572
4	COLO 205	Human colorectal adenocarcinoma; ATCC CCL-222
5	PANC-1	Human pancreatic carcinoma; ATCC CRL-1469
6	MCF-7	Human breast adenocarcinoma; ATCC HTB-22
7	SW620	Human colorectal adenocarcinoma; ATCC CCL-227
8	HCT116/p53-	HCT116 cell line with knockout of p53 gene (see Experimental Procedures)
9	HS 578T	Human breast carcinoma; ATCC HTB-126
10	PA-1/E6	PA-1 cell line expressing the herpesvirus E6 protein to inactivate p53 (see Experimental Procedures)
11	MCF-10A	Human breast epithelial cell line; ATCC CRL-10317 (not tumorigenic)
Drugs		
Sorafenib		Also known as Nexavar. Kinase inhibitor; targets multiple intracellular (CRAF, BRAF and mutant BRAF) and cell surface kinases (KIT, FLT-3, VEGFR-2, VEGFR-3, and PDGFR-β). SID:789424
Gefitinib		Iressa; epidermal growth factor receptor tyrosine kinase inhibitor.
Gleevec		Also known as Imatinib. Kinase inhibitor; targets c-Kit and other kinases. SID:841977
MCP-1		Ras-Raf interaction inhibitor, SID: 7979866
taxol		Paclitaxel; stabilizes microtubules by preventing depolymerization, leading to mitotic arrest. Paclitaxel also induces apoptosis by binding to Bcl-2. SID:177831.